Nonlinear Stall Flutter and Divergence Analysis of Cantilevered Graphite/Epoxy Wings

Peter Dunn* and John Dugundji†
Massachusetts Institute of Technology, Cambridge, Massachusetts 02139

The nonlinear, stalled, aeroelastic behavior of rectangular, graphite/epoxy, cantilevered wings with varying amount of bending-torsion stiffness coupling is investigated. A nonlinear aeroelastic analysis is developed using the nonlinear, stalled ONERA aerodynamic model initially presented by Tran and Petot. Nonlinear flutter calculations are carried out using Fourier analysis to extract the harmonics from the ONERA aerodynamics, then a harmonic balance method and a Newton-Raphson solver are applied to the resulting nonlinear, Rayleigh-Ritz aeroelastic formulation. Test wings were constructed and subjected to wind-tunnel tests for comparison against the developed analysis. Wind-tunnel tests show reasonable agreement between theory and experiment for static deflections, for linear flutter and divergence, and for nonlinear, torsional stall flutter and bending stall flutter limit cycles. The current nonlinear analysis shows a transition from divergence to bending stall flutter, which linear analyses are unable to predict.

Nomenclature

a_{oz} = linear aerodynamic slope, $\equiv dC_{zl}/d\alpha$
b = semichord, $\equiv c/2$
C_D, C_L, C_M = drag, lift, and moment coefficients, respectively
C_z = general aerodynamic coefficient; i.e., C_D, C_L, or C_M
C_{z1} = linear contribution to C_z
C_{z2} = nonlinear contribution to C_z
c = chord length
D_{ij} = flexural modulus components
h = 1/4-chord tip deflection
$\bar{h}$ = nondimensional deflection, $\equiv h/b$
K_{ij} = components of the stiffness matrix
k = reduced frequency, $\equiv \omega b/U$
l = semispan
M_{ij} = components of the mass matrix
m = mass per unit area
Q_i = ith modal force
q_i = ith modal amplitude
t = real time
U = freestream velocity
w = out-of-plane deflection
x, y, z = cartesian coordinates
α = effective angle of attack
γ_i = ith mode shape
ΔC_z = nonlinear aerodynamic force deviation
θ = instantaneous angle of attack
θ_R = root angle of attack
ρ = freestream air density
τ = nondimensional time, $\equiv Ut/b$
χ_i, ψ_i = spanwise and chordwise mode shape, respectively
φ = nondimensional phase, $\equiv k\tau + \xi$
ω = frequency

Subscripts

o, s, c = mean, sine, and cosine components, respectively
v = amplitude of oscillation

Received April 2, 1990; presented as Paper 90-0983 at the AIAA/ASME/ASCE/AHS/ASC Structures, Structural Dynamics, and Materials Conference, Long Beach, CA, April 2-4, 1990; revision received Nov. 2, 1990; accepted for publication Nov. 16, 1990.

*Research Assistant, Department of Aeronautics and Astronautics. Member AIAA.

†Professor, Department of Aeronautics and Astronautics. Member AIAA.

Introduction

MOST analysis of aircraft flutter behavior is traditionally based on small amplitude, linear theory, particularly with regards to the aerodynamic modeling. However, if the wing is near the stall region, a nonlinear stall flutter limit cycle may occur at a lower velocity than linear theory would suggest (see, for example, early work by Rainey[1]). Since some current aircraft are achieving high angle of attack for maneuvering, it is of interest to explore this nonlinear stall flutter behavior and its transition from linear behavior.

In previous investigations at Massachusetts Institute of Technology (MIT), the aeroelastic flutter and divergence behavior of cantilevered, unswept and swept, graphite/epoxy wings was investigated in a small, low-speed wind tunnel.[2-4] The wings were six-ply, graphite/epoxy plates with strong bending-torsion coupling. Experiments were conducted to determine the flutter boundaries of these wings both at low and high angles of attack, stall flutter often being observed at the latter. The divergence and flutter results at low angles of attack correlated well with linear, unsteady theory, indicating some beneficial effects of ply orientation in aeroelastic behavior,[2-4] and some static, nonlinear aerodynamics correlated well before the onset of flutter. No nonlinear, unsteady analyses were attempted for the higher angles of attack.

Recently, Tran and Petot[5] and Dat and Tran[6] of the Office National d'Etudes et de Recherches Aérospatiales (ONERA) developed a semiempirical, unsteady, nonlinear model (called the ONERA model) for determining two-dimensional aerodynamic forces on an airfoil oscillating in pitch only, which experiences dynamic stall. It was felt that this model, as amended for pitch and translation by Peters[7] and by Petot and Dat,[8] could provide a convenient means of including nonlinear stalled air forces into an analytic study of stall flutter.

The objectives of the current investigation were to develop a simple analytic aeroelastic model, using the ONERA model as the basis for the aerodynamics, to predict general characteristics of three-dimensional, stalled, flutter limit cycles while concurrently developing an experimental base of both small-amplitude and large-amplitude flutter data for a variety of composite laminate wings with a wide range of bending-tor-

sion coupling characteristics. The present investigation is described more fully in Ref. 9.

Analytical Method

Generalized Rayleigh-Ritz Problem

The layout of the composite wings and the sign convention are given in Fig. 1. The Rayleigh-Ritz analysis assumes a deflection shape for the lateral deflection w in terms of the modal amplitudes $q_i(t)$ as,

$$w = \sum_{i=1}^{n} \gamma_i(x,y)q_i(t) = \sum_{i=1}^{n} \phi_i(x)\psi_i(y)q_i(t) \tag{1}$$

The current flutter analysis uses one cantilever beam bending mode and one beam torsion mode, where the parameters of the bending and torsion modes are derived in the same manner as Crawley and Dugundji.[10] The symmetric stiffness coefficients K_{ij} and the symmetric mass coefficients M_{ij} were obtained from the composite plate and accompanying styrofoam fairing properties in standard fashion.

To increase the accuracy of the structural model, an empirical cubic stiffening factor was added to the stiffness of the first torsional mode, given by,

$$K_{22} = K_{22}^{L} + K_{22}^{C}q_2^2 \tag{2}$$

The modal forces Q_i resulting from the applied load $f(x,y)$ are defined as,

$$Q_i = \int\int_A f(x,y)\gamma_i(x,y)\mathrm{d}A \tag{3}$$

Applying Lagrange's equations of motion[11] yields the differential equations in matrix form,

$$[M]\{\ddot{q}\} + [K]\{q\} = \{Q\} \tag{4}$$

The formulation of the mass M_{ij} and stiffness K_{ij} components were verified through static deflection and free vibration experiments. For the static deflection test, a known concentrated bending load or torsion load was applied to the tip of the wing and the deflections and twist were measured and compared with the analysis. For the free vibration test, a small load was applied to the wing so as to excite free vibration, and the resulting free vibration frequencies and mode shapes were compared with the analysis.

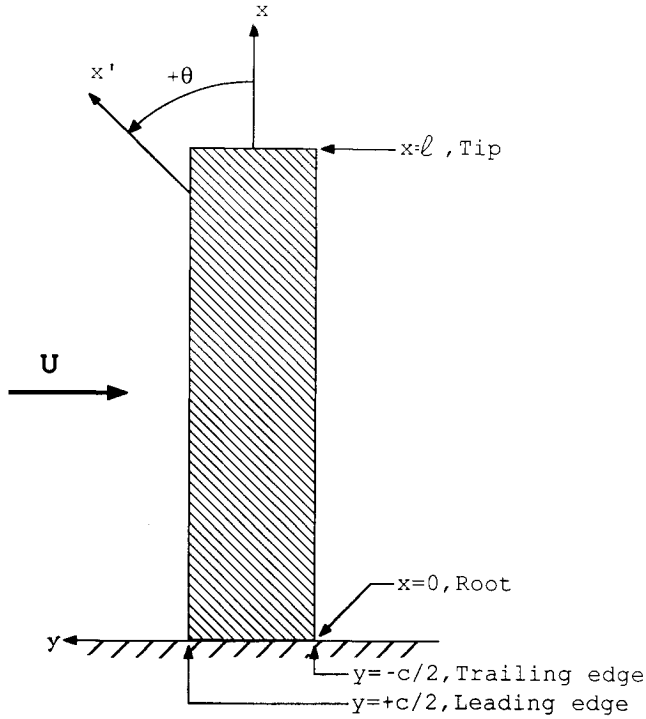

Fig. 1 Sign convention for ply angle and axes.

Aerodynamic Model

The ONERA aerodynamic model[5-8] used for this study incorporates a single lag term operating on the linear part of the airfoil's static force curve (thus analogous to a Theodorsen function approximation for linear theory) and a two lag term operating on the nonlinear (i.e., stalling) portion of the airfoil's static force curve. The ONERA model can be expressed as the sum of a linear and nonlinear part as,

$$C_z = C_{z1} + C_{z2} \tag{5}$$

$$C_{z1} = s_z\overset{*}{\alpha} + k_{vz}\overset{*}{\theta} + C_{z\gamma} \tag{6}$$

$$\overset{*}{C}_{z\gamma} + \lambda_z C_{z\gamma} = \lambda_z[a_{oz}\alpha + \sigma_z\overset{*}{\theta}] + \alpha_z[a_{oz}\overset{*}{\alpha} + \sigma_z\overset{**}{\theta}] \tag{7}$$

$$\overset{**}{C}_{z2} + 2dw\overset{*}{C}_{z2} + w^2(1+d^2)C_{z2} = = -w^2(1+d^2)\left[\Delta C_z|_\alpha + e\frac{\partial \Delta C_z}{\partial \tau}|_\alpha\right] \tag{8}$$

where

$$\alpha = \theta - \overset{*}{h} \tag{9}$$

$$(*) \equiv \frac{\partial(\,)}{\partial \tau}, \qquad \tau \equiv Ut/b \tag{10}$$

where s_z, k_{vz}, λ_z, σ_z, α_z, w, d, and e are the coefficients associated with the appropriate force coefficient, which are determined empirically by parameter identification,[12-14] and are listed in Table 1. The deviation ΔC_z is defined as positive for a decrease in the aerodynamic force, as shown in Fig. 2, and it yields the static aerodynamic force curve,

$$C_{zs}(\alpha) = a_{oz}\alpha - \Delta C_z(\alpha) \tag{11}$$

In the current study, the deviation ΔC_z is defined by simple straight line fits between discrete points. Thus, the three-dimensional force coefficients were determined by empirically fitting two-dimensional data from Jacobs and Sherman[13] for this $AR = 8$ wing and are given by,

$$\begin{aligned} C_L &= 1.11[1 - (x/l)^9][4.7^*\alpha]; \qquad \alpha \le 0.175 \text{ (10 deg)} \\ &= 1.11[1 - (x/l)^9][0.82 - 0.4(\alpha - .175)]; \\ &\qquad 0.175 \le \alpha \le 0.349 \\ &= 1.11[1 - (x/l)^9]^*0.75; \qquad \alpha \ge 0.349 \text{ (20 deg)} \end{aligned} \tag{12}$$

$$\begin{aligned} C_M &= 0.0; \qquad \alpha \le 0.175 \text{ (10 deg)} \\ &= 1.11[1 - (x/l)^9][-0.62^*(\alpha - 0.175)]; \\ &\qquad 0.175 \le \alpha \le 0.349 \\ &= 1.11[1 - (x/l)^9][-0.108 - 0.14(\alpha - 0.349)]; \\ &\qquad \alpha \ge 0.349 \text{ (20 deg)} \end{aligned} \tag{13}$$

$$C_D = 4.923\alpha^3 + 0.1473\alpha^2 + 0.042\alpha + 0.014 + C_L^2/\pi AR \tag{14}$$

where the angle of attack α is expressed in radians. For greater accuracy, the ΔC_z can be described more generally by polyno-

Table 1 Coefficients of aerodynamic equations

Quantity	Lift	Moment
a_{oz}	5.9 rad^{-1}	0
s_z	0.09(180/π) rad^{-1}	$-\pi/4$ rad^{-1}
k_{vz}	$\pi/2$ rad^{-1}	$-3\pi/16$ rad^{-1}
λ_z	0.15	0
α_z	0.55	1
σ_z	5.9 rad^{-1}	$-\pi/4$ rad^{-1}
a^a	$0.25+0.1(\Delta C_L)^2$	
a^b	$0.25+0.4(\Delta C_L)^2$	
r^a	$[0.2+0.10(\Delta C_L)^2]^2$	
r^b	$[0.2+0.23(\Delta C_L)^2]^2$	
d	$a/\sqrt{4r-a^2}$	
w	$a/2d$	
e^a	$-0.6(\Delta C_L)^2$	
e^b	$-2.7(\Delta C_L)^2$	

[a]If $Re>3.4\times10^5$. [b]If $Re<3.4\times10^5$.

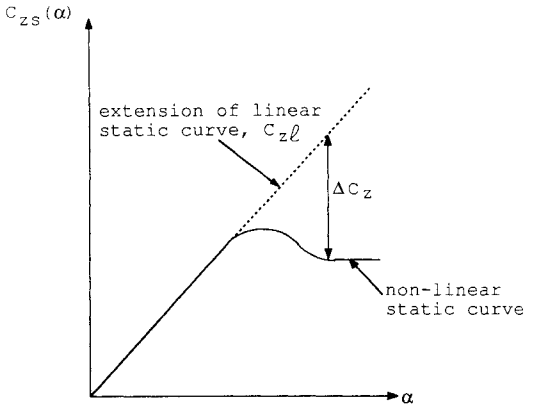

Fig. 2 Description of static aerodynamic curve.

mials in several regions of the aerodynamic force curve,

$$\Delta C_z(\alpha) = \sum_{j=0}^{J_i} a_{ij}(\alpha - \alpha_i)^j \tag{15}$$

for $a_i \le \alpha \le \alpha_{i+1}$ where $a_{io} \equiv \Delta C_z(\alpha_1)$ and $\Delta C_z(\alpha_1) \equiv 0$. Once the aerodynamic force coefficients are determined, they are inserted into Eq. (3) to give the modal forces,

$$Q_i = \frac{1}{2}\rho U^2 \int_0^l \left\{ c\left[C_L(x)\cos\theta_R + C_D(x)\sin\theta_R \right]\psi_i\left(+\frac{c}{4}\right) + c^2 C_M(x)\psi_{i,y}\left(+\frac{c}{4}\right)\right\}\phi_i(x)\,dx \tag{16}$$

Fourier Analysis of the Nonlinear Aerodynamics

For later use in the Harmonic Balance Method, it is necessary to evaluate the lowest-order frequency components of the nonlinear aerodynamic force coefficients when harmonic angle of attack and 1/4-chord deflection are given as inputs,

$$\theta(\tau) = \theta_o + \theta_s \sin(k\tau) + \theta_c \cos(k\tau) \tag{17}$$

$$\bar{h}(\tau) = \bar{h}_o + \bar{h}_s \sin(k\tau) + \bar{h}_c \cos(k\tau) \tag{18}$$

where $k = \omega b/U$ and $\tau = Ut/b$ are the reduced frequency and nondimensional time, respectively. Thus, the effective angle of attack α is given by,

$$\alpha(\tau) = \alpha_o + \alpha_s \sin(k\tau) + \alpha_c \cos(k\tau) \tag{19}$$

or, in purely sinusoidal form,

$$\alpha(\tau) = \alpha_o + \alpha_v \sin(k\tau + \xi) = \alpha_o + \alpha_v \sin\varphi \tag{20}$$

where

$$\alpha_o = \theta_o \tag{21a}$$

$$\alpha_s = \theta_s + k\bar{h}_c \tag{21b}$$

$$\alpha_c = \theta_c - k\bar{h}_s \tag{21c}$$

$$\alpha_v = \sqrt{\alpha_s^2 + \alpha_c^2} \tag{22a}$$

$$\xi = \sin^{-1}\frac{\alpha_c}{\alpha_v} \tag{22b}$$

$$\varphi = k\tau + \xi \tag{22c}$$

Harmonic motion is assumed for ΔC_z giving,

$$\Delta C_z(\tau) = \Delta C_{zo} + \Delta C_{zv}\sin\varphi + \text{H.H.T.} \tag{23}$$

where, as demonstrated in Fig. 3, Fourier analysis yields,

$$\Delta C_{zo} = \frac{1}{2\pi}\int_0^{2\pi} \Delta C_z(\tau)\,d\varphi = \frac{1}{\pi}\int_{-\frac{\pi}{2}}^{+\frac{\pi}{2}} \Delta C_z(\tau)\,d\varphi \tag{24}$$

$$\Delta C_{zv} = \frac{2}{\pi}\int_{-\frac{\pi}{2}}^{+\frac{\pi}{2}} \Delta C_z(\tau)\sin\varphi\,d\varphi \tag{25}$$

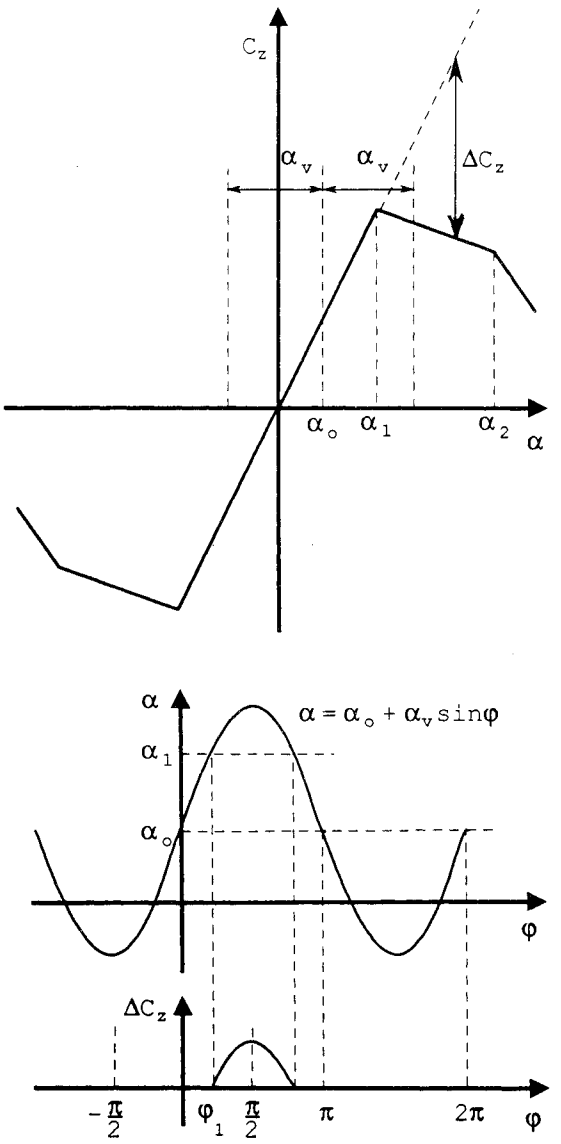

Fig. 3 Example of oscillation straddling stall angle.

Inserting the sinusoidal form of the angle of attack from Eq. (20) into the polynomial separation of ΔC_z from Eq. (15) and applying the Fourier analysis of Eqs. (24) and (25) yields,

$$\Delta C_{zo} = \frac{1}{\pi} \sum_i \sum_{m=0}^{J_i} b_{im} I_{im} \tag{26}$$

$$\Delta C_{zv} = \frac{2}{\pi} \sum_i \sum_{m=0}^{J_i} b_{im} I_{i,m+1} \tag{27}$$

where

$$b_{im} = \sum_{j=m}^{J_i} \binom{j}{m} a_{ij} \alpha_v^j \left(\frac{\alpha_o - \alpha_i}{\alpha_v}\right)^j \tag{28}$$

with

$$\binom{j}{m} = \frac{j!}{m!(j-\mathrm{m})!}$$

$$I_{im} = \int_{\varphi_i}^{\varphi_{i+1}} \sin^m\varphi \, d\varphi = \frac{-\sin^{m-1}\varphi \cos\varphi}{m} \Bigg|_{\varphi_i}^{\varphi_{i+1}} + \frac{m-1}{m} I_{i,m-2} \tag{29}$$

and the first two values of I_{im} required for the recursive formula in Eqs. (29) are,

$$I_{i0} = \int_{\varphi_i}^{\varphi_{i+1}} d\varphi = \varphi_{i+1} - \varphi_i \tag{30}$$

$$I_{i1} = \int_{\varphi_i}^{\varphi_{i+1}} \sin\varphi \, d\varphi = -\cos\varphi_{i+1} - \cos\varphi_i \tag{31}$$

The nondimensional limits of integration φ_i are

$$\varphi_i = \sin^{-1}\left(\frac{\alpha_i - \alpha_o}{\alpha_v}\right)$$

$$\varphi_i = \begin{cases} +\pi/2 & \text{if} \quad \alpha_o + \alpha_v < \alpha_i \\ -\pi/2 & \text{if} \quad \alpha_o - \alpha_v > \alpha_i \end{cases} \tag{32}$$

ΔC_z is then converted from purely sinusoidal form [Eq. (23)] to the usual sine and cosine harmonic form,

$$\Delta C_z(\tau) = \Delta C_{zo} + \Delta C_{zs} \sin(k\tau) + \Delta C_{zc} \cos(k\tau) \tag{33}$$

where

$$\Delta C_{zs} = \Delta C_{zv} \cos\xi = \Delta C_{zv} \frac{\alpha_s}{\sqrt{\alpha_s^2 + \alpha_c^2}} \tag{34}$$

$$\Delta C_{zc} = \Delta C_{zv} \sin\xi = \Delta C_{zv} \frac{\alpha_c}{\sqrt{\alpha_s^2 + \alpha_c^2}} \tag{35}$$

The time derivative of ΔC_z is given by,

$$\frac{\partial \Delta C_z(\tau)}{\partial \tau} = -k \Delta C_{zc} \sin(k\tau) + k \Delta C_{zs} \cos(k\tau) \tag{36}$$

Harmonic Balance Method

The aeroelastic problem is reduced from differential form to algebraic form by first assuming harmonic motion for the modal amplitudes,

$$q_i(\tau) = q_{io} + q_{is} \sin(k\tau) + q_{ic} \cos(k\tau) \tag{37}$$

The angle of attack and 1/4-chord deflection, required in Eqs. (17) and (18), are readily determined from the modal amplitudes,

$$\bar{h}(x,\tau) = \bar{h}_o(x) + \bar{h}_s(x) \sin(k\tau) + \bar{h}_c(x) \cos(k\tau) \tag{38}$$

$$\theta(x,\tau) = \theta_o(x) + \theta_s(x) \sin(k\tau) + \theta_c(x) \cos(k\tau) \tag{39}$$

where

$$\bar{h}_o(x) = \sum_{i=1}^{n} \frac{q_{io}}{b} \phi_i(x) \psi_i(+c/4) \tag{40}$$

$$\theta_o(x) = \theta_{\text{root}} + \sum_{i=1}^{n} q_{io} \phi_i(x) \psi_{i,y}(+c/4) \tag{41}$$

$$\bar{h}_s, \ \bar{h}_c, \ \theta_s, \ \theta_c = \text{etc}$$

The circulatory terms of the linear aerodynamics are given by

$$C_{z\gamma}(x,\tau) = C_{z\gamma o}(x) + C_{z\gamma s}(x) \sin(k\tau) + C_{z\gamma c}(x) \cos(k\tau) \tag{42}$$

where

$$C_{z\gamma o}(x) = a_{oz} \theta_o(x) \tag{43}$$

$$C_{z\gamma s}(x) = F(k) L_s(x) - G(k) L_c(x) \tag{44}$$

$$C_{z\gamma c}(x) = G(x) L_s(x) + F(k) L_c(x) \tag{45}$$

The F and G functions are the resulting single lag approximations to the Theodorsen function, $C(k) = F(k) + iG(k)$, namely,

$$F(k) = \frac{\lambda_z^2 + \alpha_z k^2}{\lambda_z^2 + k^2} \tag{46}$$

$$G(k) = -\frac{\lambda_z k (1 - \alpha_z)}{\lambda_z^2 + k^2} \tag{47}$$

and one has also that,

$$L_s(x) = a_{oz}[\theta_s(x) + k\bar{h}_c(x)] - \sigma_z k \theta_c(x) \tag{48}$$

$$L_c(x) = a_{oz}[\theta_c(x) - k\bar{h}_s(x)] + \sigma_z k \theta_s(x) \tag{49}$$

Adding the apparent mass terms to the circulatory terms gives the linear contribution to the aerodynamics,

$$C_{z1o}(x) = C_{z\gamma o}(x) \tag{50}$$

$$C_{z1s}(x) = C_{z\gamma s}(x) - s_z[k\theta_c(x) - k^2\bar{h}_s(x)] - k_{vz} k^2 \theta_s(x) \tag{51}$$

$$C_{z1c}(x) = C_{z\gamma c}(x) + s_z[k\theta_s(x) - k^2\bar{h}_c(x)] - k_{vz} k^2 \theta_c(x) \tag{52}$$

The nonlinear contribution to the aerodynamics is

$$C_{z2}(x,\tau) = C_{z2o}(x) + C_{z2s}(x) \sin(k\tau) + C_{z2c}(x) \cos(k\tau) \tag{53}$$

where

$$C_{z2o}(x) = -\Delta C_{zo}(x) \tag{54}$$

$$C_{z2s}(x) = \frac{K_1 K_3 + K_2 K_4}{K_1^2 + K_2^2} \tag{55}$$

$$C_{z2c}(x) = \frac{K_1 K_4 - K_2 K_3}{K_1^2 + K_2^2} \tag{56}$$

and one has the intermediate variables,

$$K_1 = 1 + d^2 - \left(\frac{k}{w}\right)^2 \tag{57}$$

$$K_2 = 2d\frac{k}{w} \tag{58}$$

$$K_3 = -(1 + d^2)[\Delta C_{zs}(x) - ek\Delta C_{zc}(x)] \quad (59)$$

$$K_4 = -(1 + d^2)[\Delta C_{zc}(x) + ek\Delta C_{zs}(x)] \quad (60)$$

The linear and nonlinear contributions are then combined to give the total aerodynamic force components,

$$C_z(x, \tau) = C_{zo}(x) + C_{zs}(x)\sin(k\tau) + C_{zc}(x)\cos(k\tau) \quad (61)$$

where

$$C_{zo}(x) = C_{z1o}(x) + C_{z2o}(x) \quad (62)$$

$$C_{zs},\ C_{zc} = \text{etc}$$

Finally, these harmonic components of the aerodynamic forces are used to formulate the harmonic components of the modal forces as,

$$Q_i(\tau) = Q_{io} + Q_{is}\sin(k\tau) + Q_{ic}\cos(k\tau) \quad (63)$$

where,

$$Q_{io} = \frac{1}{2}\rho U^2 \int_0^l \{c[C_{Lo}(x)\cos\theta_R + C_{Do}(x)\sin\theta_R]\psi_i(+\frac{c}{4}) + c^2 C_{Mo}(x)\psi_{i,y}(+\frac{c}{4})\phi_i(x)\,dx \quad (64)$$

$$Q_{is},\ Q_{ic} = \text{etc}$$

Combining the harmonic form of the modal amplitudes with the harmonic form of the modal forces yields the nonlinear matrix equation,

$$\begin{bmatrix} [K] & 0 & 0 \\ 0 & -\omega^2[M] + [K] & 0 \\ 0 & 0 & -\omega^2[M] + [K] \end{bmatrix} \begin{bmatrix} \{q_o\} \\ \{q_s\} \\ \{q_c\} \end{bmatrix} = \begin{bmatrix} \{Q_o\} \\ \{Q_s\} \\ \{Q_c\} \end{bmatrix} \quad (65)$$

Matrix equation (65) is solved via a Newton-Raphson method. To ensure that a nontrivial flutter solution is reached, the sine component of one of the modes (usually the first torsion mode) is set to a desired amplitude and the cosine component of the same mode is set to zero. The problem statement still retains the same number of unknown variables as equations since the Newton-Raphson solver must still solve for the remaining modal amplitudes as well as the unknown reduced frequency of oscillation and the unknown flutter velocity. This is similar to the procedure used for nonlinear panel flutter by Kuo et al.[15]

Experiment

Test specimens were constructed from AS4/3501-6 graphite/epoxy cut to dimensions of 330 × 76.2 mm (13 × 3 in.). Loading tabs, bending and torsion strain gauges, and styrofoam fairings were affixed as shown in Fig. 4. $[0_2/90]_s$, $[+15_2/0]_s$, and $[-15_2/0]_s$ laminate layups were constructed. The airfoil shape of the styrofoam fairings was a NACA 0012.

Wind-tunnel tests were conducted in the MIT Department of Aeronautics and Astronautics acoustic wind tunnel with a 1.5- × 2.3-m (5- × 7.5-ft) free jet test section, 2.3 m (7.5 ft) long. The test setup, shown in Fig. 5, involved mounting the wing specimen vertically on a rotating stand. Data was taken both through bending and torsion strain gauge readings recorded onto a Digital Oscilloscope and by recording tip deflections onto videotape by viewing via an overhead mirror.

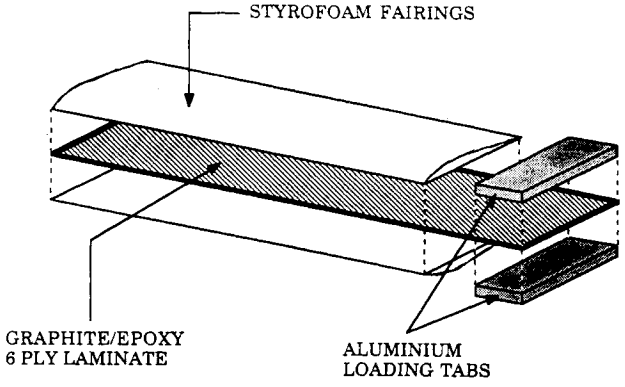

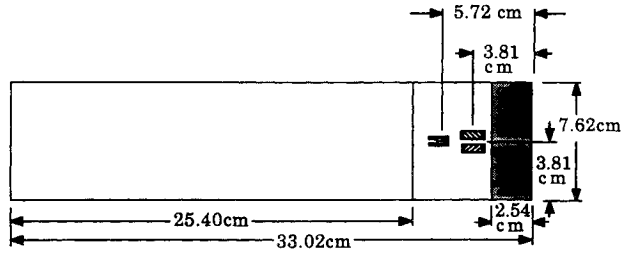

Fig. 4 Wing construction and dimensions.

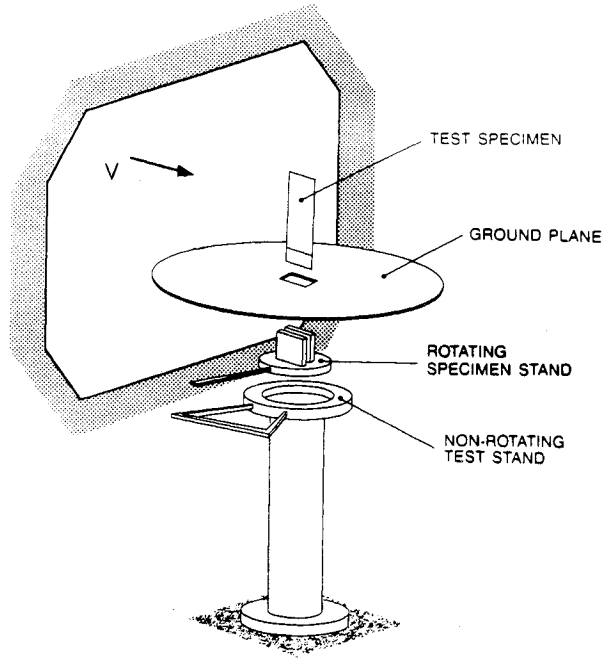

Fig. 5 Wind-tunnel setup.

For a wide range of root angles of attack varying from zero to almost twice the static stall angle, static deflection data was recorded over a range of velocities below the flutter velocity, and unsteady deflection data was recorded both at and above the flutter velocity.

Results

Natural vibration frequencies for the NACA 0012 wings were determined both experimentally and analytically (using a five-mode Rayleigh-Ritz analysis for greater accurcy) and are tabulated in Table 2. Although these are listed as first bending (1B), first torsion (1T), and second bending (2B), with highly coupled laminates this distinction becomes much less meaningful because of the high bending-torsion coupling. The experimental frequencies show good agreement with the analysis

Table 2 Free vibration frequencies of NACA 0012 wings

	Experiment, Hz			Analysis, Hz		
Layup	1B	1T	2B	1B	1T	2B
$[0_2/90]_s$	9.9	50.1	63.2	10.5	51.2	66.1
$[+15_2/0]_s$	8.8	52.8	61.9	9.1	52.4	65.1
$[-15_2/0]_s$	8.6	52.1	61.4	9.1	52.4	65.1

Table 3 Linear divergence and flutter values

Layup	Divergence velocity, m/s	Flutter velocity, m/s	Flutter frequency, Hz
$[0_2/90]_s$	38.1	36.4	25.8
$[+15_2/0]_s$	>50	37.3	27.3
$[-15_2/0]_s$	21.6	48.8	29.7

for the bending modes and the first torsional mode. The vibration results indicate that the styrofoam fairing stiffens the wings in torsion, but comparatively little in bending.

Two-Dimensional Aerodynamics

Experimental results of two-dimensional lift coefficient and moment coefficient hysteresis loops from McAlister et al.[16] for a NACA-0012 airfoil in low Reynolds number flow are compared against analysis, using the two lowest harmonics, in Fig. 6. The lift hysteresis loops show fair agreement between experiment and theory, whereas the moment hysteresis loops seem to show poor agreement. However, these discrepancies in the moment loops may be overlooked in the subsequent analysis since the moment hysteresis loops contain a large component of higher frequencies, and it is the lowest harmonic component that is of importance for the analysis here. Also, the moment generated by the lift at the 1/4 chord will generally offset the moment generated around the 1/4 chord.

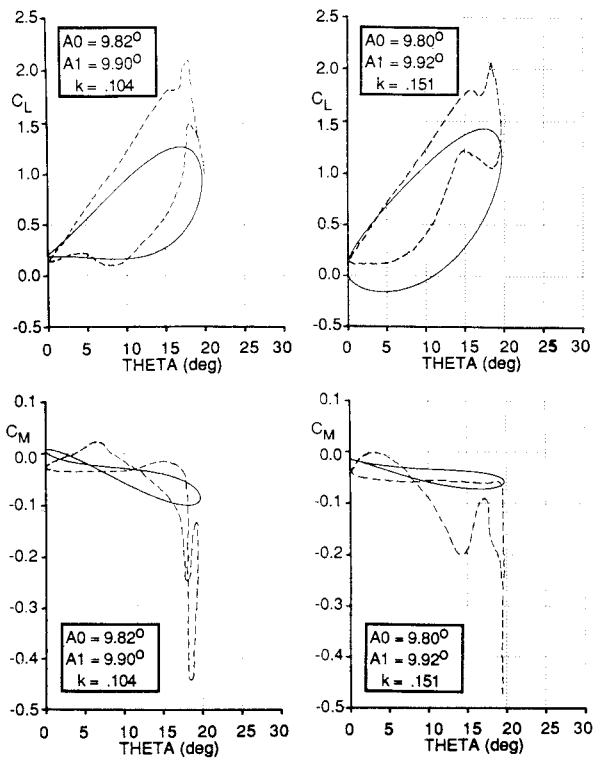

Fig. 6 Two-dimensional aerodynamic loops compared vs Ref. 16: —— analysis; --- experiment.

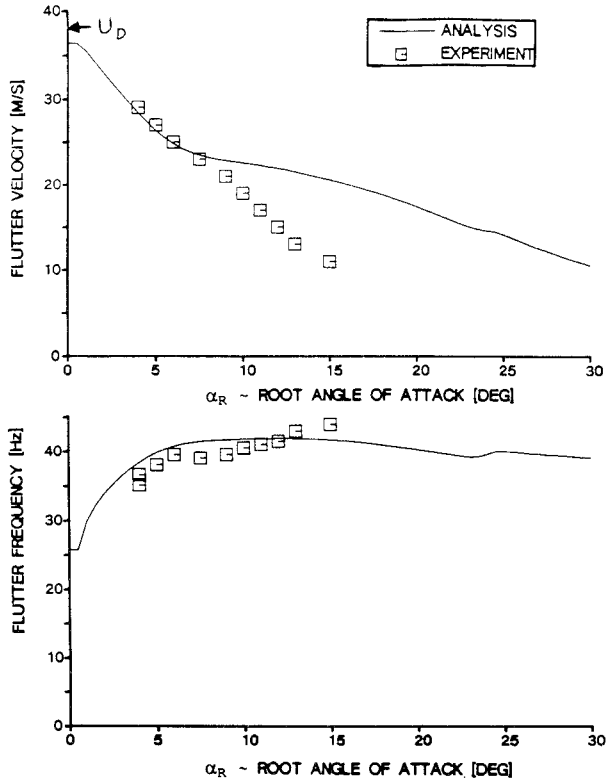

Fig. 7 $[0_2/90]_s$ flutter boundary and frequency variation.

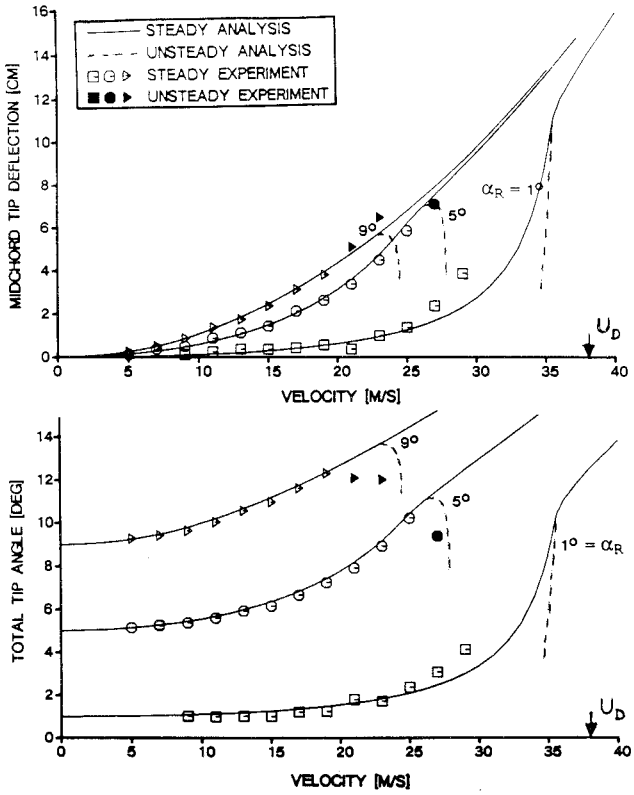

Fig. 8 $[0_2/90]_s$ averaged tip deflection and angle.

Flutter Results

The linear flutter and divergence characteristics were determined both by applying the standard *U-g* method and also by turning off all of the nonlinear aerodynamics in the harmonic balance method discussed here. The results of the linear analysis are listed in Table 3.

The flutter boundary for the $[0_2/90]_s$ wing (Fig. 7) shows a very short range of linear behavior because the divergence

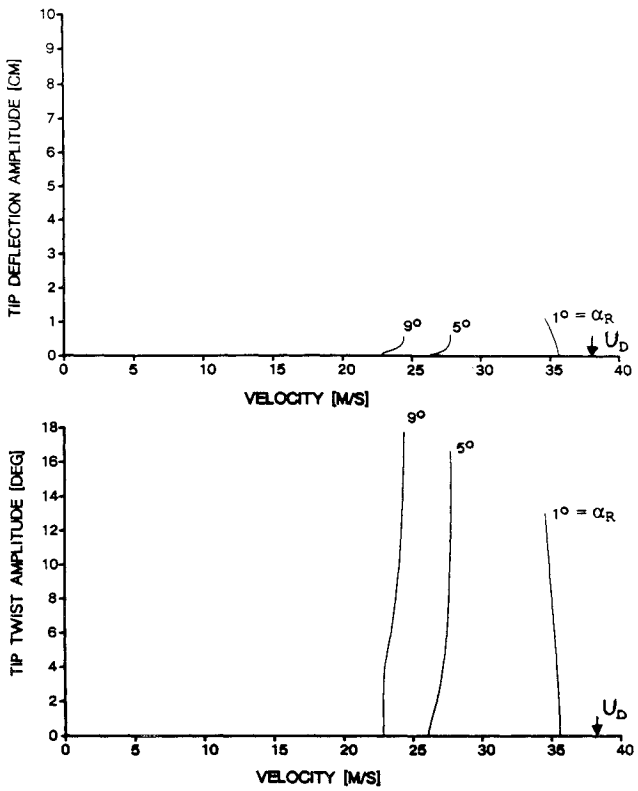

Fig. 9 $[0_2/90]_s$ deflection and angle oscillation amplitudes.

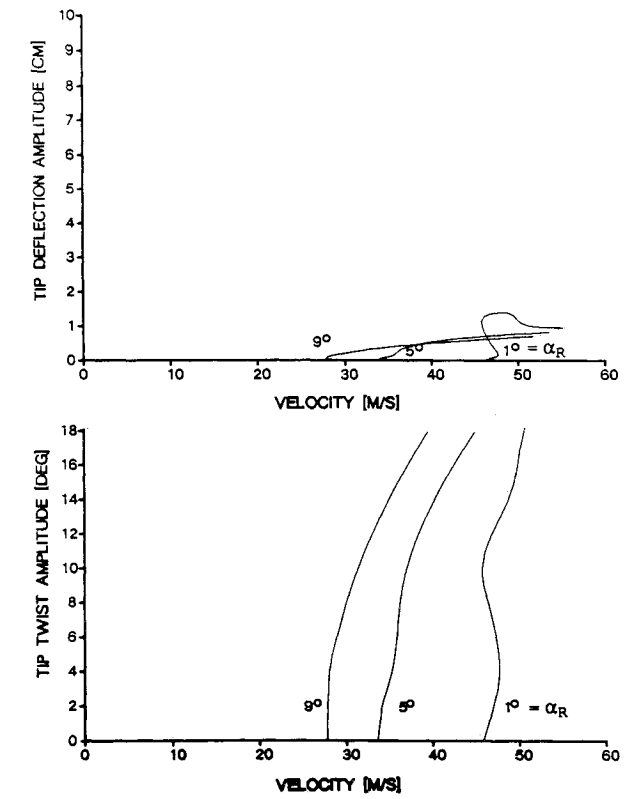

Fig. 10 $[0_2/90]_s$ deflection and angle oscillation amplitudes (cubic stiffening included).

velocity is very near the flutter velocity, thus driving the wing very quickly into the nonlinear stall range. After this linear range, an increase in the root angle of attack causes the flutter velocity to drop and the flutter motion to become more purely torsional (denoted by a frequency closer to the first-torsion free vibration frequency and a decrease in the bending amplitude). This decreased flutter speed with increased angle of attack was also noted by Rainey[1] for isotropic wings. The nonlinear analysis in Fig. 7 compares reasonably with the experimental flutter boundaries and flutter frequencies.

The analysis without cubic stiffening in Fig. 8 for the $[0_2/90]_s$ wing indicates the strong interaction of static tip angle with stall flutter. The midchord tip deflection and total tip angle exhibit a sharp decrease when the velocity is increased past the flutter boundary. The experimental trend actually

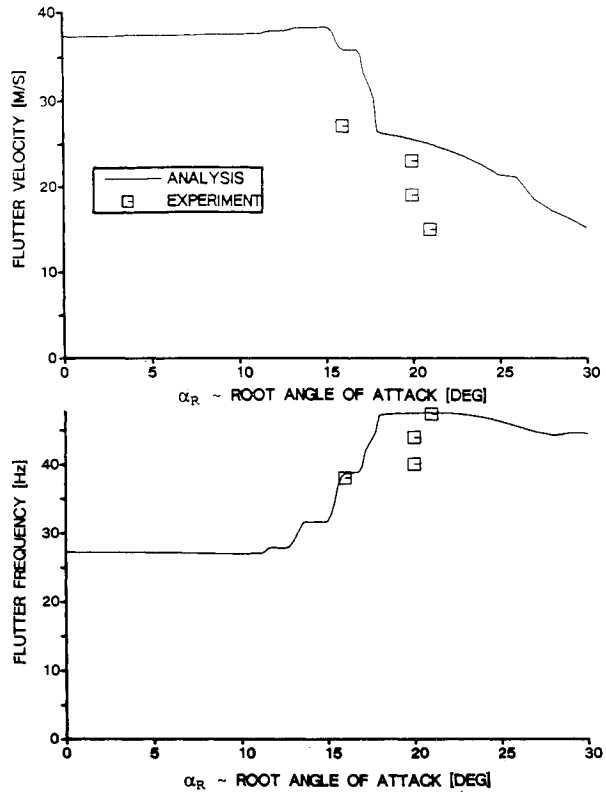

Fig. 11 $[+15_2/0]_s$ flutter boundary and frequency variation.

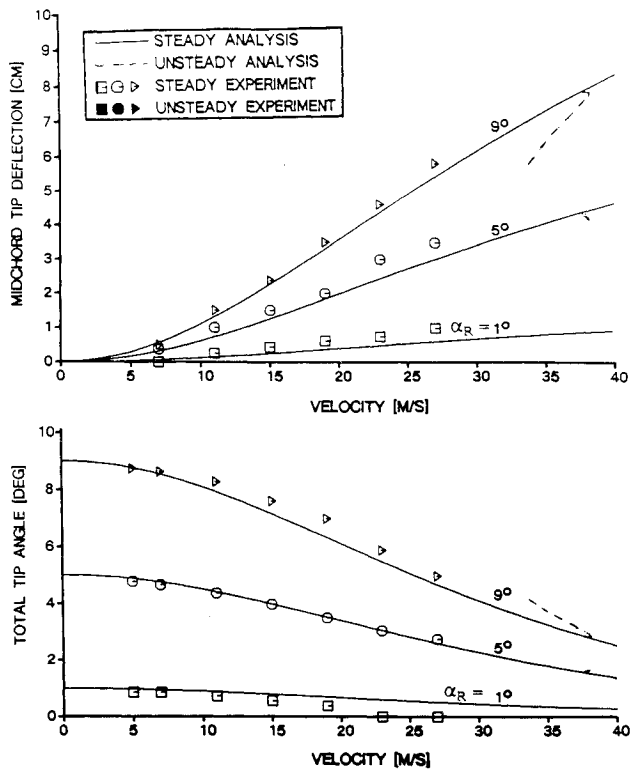

Fig. 12 $[+15_2/0]_s$ averaged tip deflection and angle.

exhibits an increase in midchord tip deflection while the tip angle decreases in agreement with the analytic trend. The analytic results in Fig. 9 demonstrate the high torsional content of this flutter since little bending motion is present.

The analysis with cubic stiffening is shown in Fig. 10. (Analysis with cubic stiffening was only conducted for the $[0_2/90]_s$ wing.) Without cubic stiffening, the analysis in Fig. 9 demonstrates some softening effects from the nonlinear aerodynamics; that is, increasing amplitudes of oscillation could be analytically achieved by reducing the freestream velocity, and correspondingly no analytic solution exists above the flutter velocity. This trend runs counter to the experimental results, where the amplitudes of oscillation increase with increasing freestream velocity. However, as seen in Fig. 10, with the cubic stiffening included in the structural analysis, the amplitude of oscillation now increases with increasing velocity.

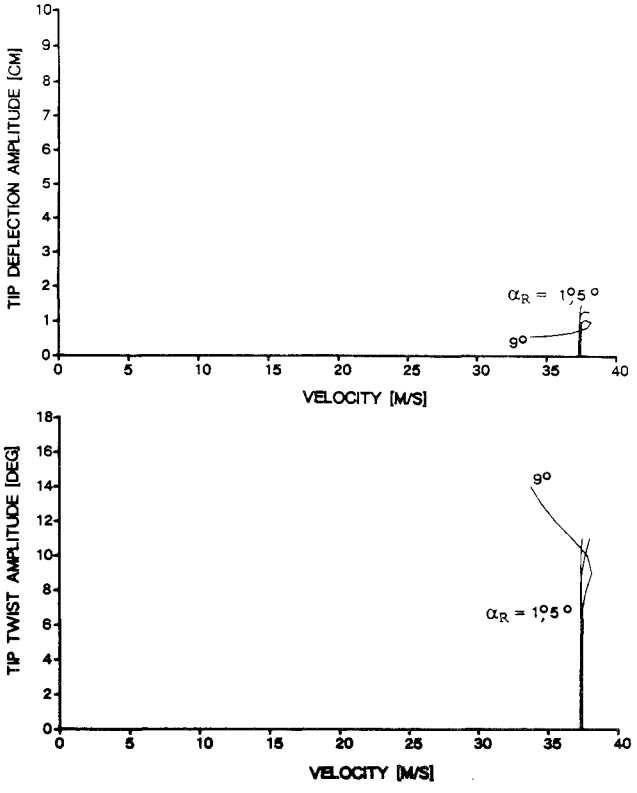

Fig. 13 $[+15_2/0]_s$ deflection and angle oscillation amplitudes.

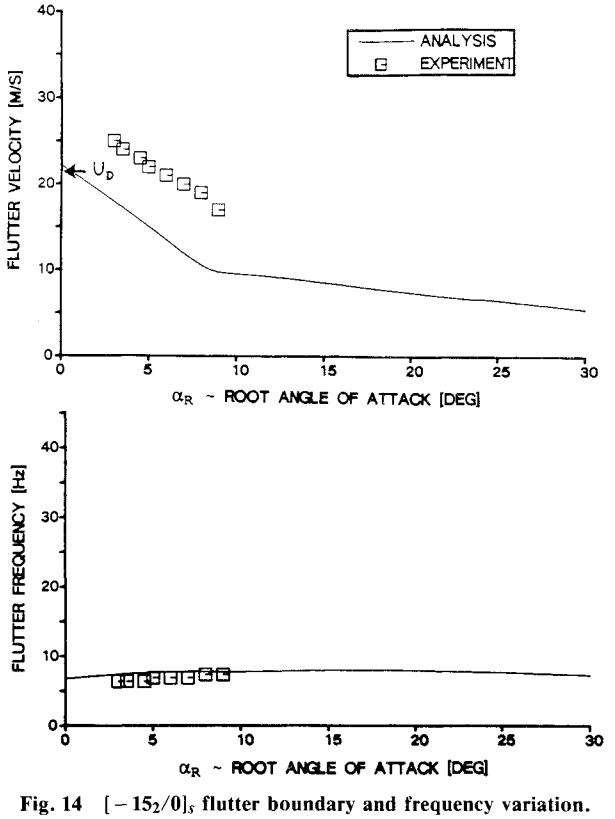

Fig. 14 $[-15_2/0]_s$ flutter boundary and frequency variation.

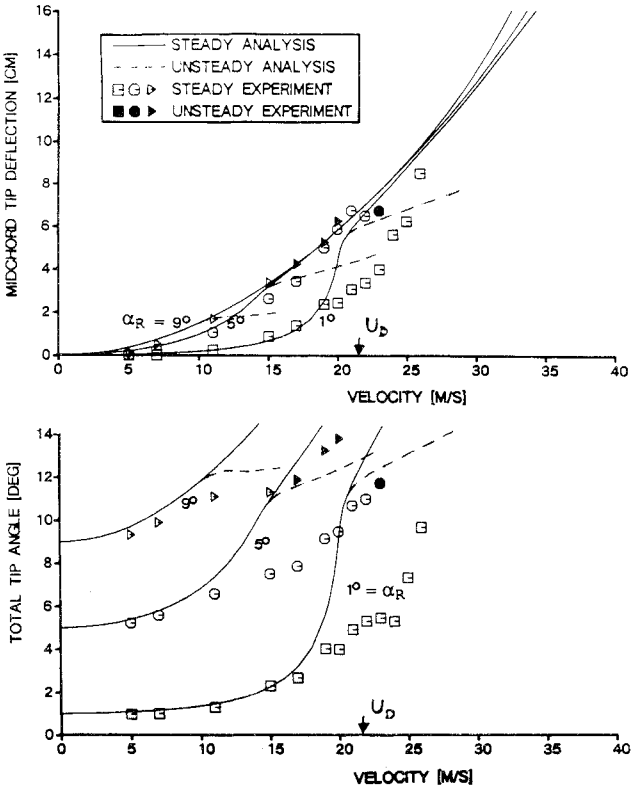

Fig. 15 $[-15_2/0]_s$ averaged tip deflection and angle.

The $[+15_2/0]_s$ wing (negative bending-twist coupling, i.e., upward wing deflection decreases the angle of attack) has a torsional flutter velocity just above that of the $[0_2/90]_s$ wing and does not experience divergence. The flutter bound for the $[+15_2/0]_s$ wing, Fig. 11, shows a more extended range of linear behavior than the $[0_2/90]_s$ wing (since the wingtip tends to twist downward and delay reaching the stall region) and a very sharp change in the flutter behavior once it goes into the nonlinear stall region. Limitations in the wind-tunnel velocity precluded taking experimental data in the linear range for the $[+15_2/0]_s$ wing, although the nonlinear analysis compares reasonably in Fig. 11. An analytic softening trend in the flutter characteristics is seen in Figs. 12 and 13 for the $[+15_2/0]_s$ wing: that is, a decrease in velocity will increase the flutter amplitude. Again, the upper limit on the velocity of the wind tunnel precluded investigating any of this phenomenon experimentally. Trends similar to those of the $[0_2/90]_s$ wing might be expected if the cubic stiffening effects were included in the analysis.

The $[-15_2/0]_s$ wing (positive bending-twist coupling, i.e., upward wing deflection increases the angle of attack) has a divergence velocity well below its torsional flutter velocity. The flutter boundary for the $[-15_2/0]_s$ wing, Fig. 14, indicates a much different trend than the mostly torsional flutter exhibited by the $[0_2/90]_s$ and $[+15_2/0]_s$ wings: the flutter is characterized by a low, first-bending frequency and immediate nonlinear, bending stall flutter in the range of the divergence velocity. There is no portion of the flutter graph here that could have been predicted by a linear analysis. The nonlinear analysis in Fig. 14 for the $[-15_2/0]_s$ compares reasonably with experiment when one considers that the analysis and

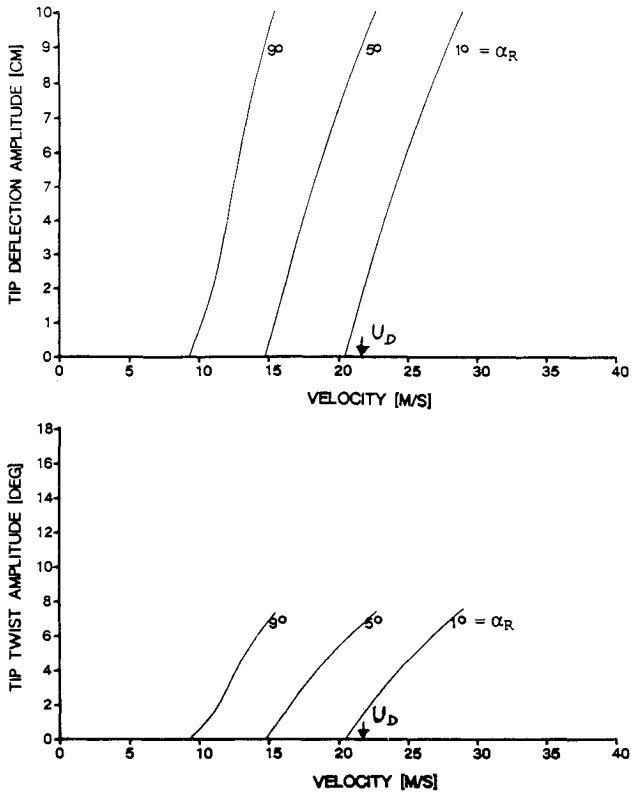

Fig. 16 $[-15_2/0]_s$ deflection and angle oscillation amplitudes.

experiment both indicate a bending flutter frequency, that they both display the same trend for flutter velocity, only shifted by a few m/s, and that more discrepancy is expected for the $[-15_2/0]_s$ wing since it reaches the nonlinear regime more quickly due to the divergence. Figure 15 for the $[-15_2/0]_s$ wing shows a more gentle deviation from the steady analysis, as compared to the sharp change in character demonstrated by the $[0_2/90]_s$ wing. Figure 16, showing the amplitude of oscillation of the bending and torsion components, displays a much higher bending component, as would be expected for this predominantly bending stall flutter. Again, as with the flutter boundary for the $[-15_2/0]_s$ wing, analysis and experiment in Figs. 15 and 16 show similar trends.

Conclusions

The present paper has presented a simple analytic method to include nonlinear structural and aerodynamic effects into a stall flutter analysis, so that these nonlinear effects can be better understood. As an alternative to using an extensive computational fluid-dynamic procedure (see, for example, Wu et al.[17]), the present analysis applies the mathematical tools of Fourier analysis, harmonic balance and the Newton-Raphson method as a numerical solver. The method makes use of a cubic torsional stiffness model together with the nonlinear ONERA stall flutter model for the aerodynamics. The current analysis presents a large step forward from previous linear analyses and allows for a broader range of nonlinear problems to be considered.

Experimental data have been obtained on a set of aeroelastically tailored wings with varying amounts of bending-torsion coupling. These matched the trends of previous studies and were used to correlate the formulated nonlinear analysis.

The current nonlinear aeroelastic analysis predicts reasonably almost all the observed, experimental, nonlinear stall phenomena on the wings tested. Specifically, limit cycle amplitudes at flutter have been obtained, and flutter boundaries have been found that decrease with root angle of attack. The transitions from linear, coupled-mode, bending-torsion flutter to predominantly single mode, torsional stall flutter, and from linear divergence to bending stall flutter, have been predicted analytically. Although the wings in this experimental study were relatively flexible, it is hoped that the present nonlinear analysis and experiments have given some insight into the stall behavior of wings at high angles of attack.

Appendix—Example of Fourier Analysis

For a single break point model, for which $i = 1$ and $J_i = 1$, Eq. (15) simplifies to the following equations, where α_1 is the stall angle and a_{11} is the difference in slopes between the linear region and the nonlinear region,

$$\Delta C_z = a_{11}(\alpha - \alpha_1) \qquad \text{for } \alpha \geq \alpha_1$$
$$= 0 \qquad \text{for } \alpha \leq \alpha_1 \tag{A1}$$

Equations (28-32) then give that,

$$b_{10} = a_{11}(\alpha_o - \alpha_1) \tag{A2}$$

$$b_{11} = a_{11}\alpha_v \tag{A3}$$

$$I_{10} = \frac{\pi}{2} - \varphi_1 \tag{A4}$$

$$I_{11} = \cos\varphi_1 \tag{A5}$$

$$I_{12} = \frac{1}{2}\sin\varphi_1 \cos\varphi_1 + \frac{\pi}{4} - \frac{1}{2}\varphi_1 \tag{A6}$$

where

$$\varphi_1 = \sin^{-1}\left\{\frac{\alpha_1 - \alpha_0}{\alpha_v}\right\}$$
$$= +\frac{\pi}{2} \qquad \text{if } \frac{\alpha_1 - \alpha_o}{\alpha_v} > +1$$
$$= -\frac{\pi}{2} \qquad \text{if } \frac{\alpha_1 - \alpha_o}{\alpha_v} < -1 \tag{A7}$$

Finally, putting these expressions into the combined mean and oscillatory components of the nonlinear aerodynamic deviation [Eqs. (26) and (27)], gives,

$$\Delta C_{zo} = \frac{a_{11}\alpha_v}{\pi}\left\{-\frac{\alpha_1 - \alpha_0}{\alpha_v}\left[\frac{\pi}{2} - \varphi_1\right] + \cos\varphi_1\right\} \tag{A8}$$

$$\Delta C_{zv} = \frac{a_{11}\alpha_v}{\pi}\left\{-\sin\varphi_1 \cos\varphi_1 + \frac{\pi}{2} - \varphi_1\right\} \tag{A9}$$

A symmetric aerodynamic force curve can also be accounted for by including a second stall angle at $\bar{\alpha}_1 = -\alpha_1$. This yields expanded versions of Eqs. (A8) and (A9), which now include a second term similar to each of the above which is subtracted from each expression, but with φ_1 replaced by $\bar{\varphi}_1$ and $\pi/2$ replaced by $-\pi/2$. The $\bar{\varphi}_1$ is defined by Eq. (A7) by again replacing $\varphi_1 \to \bar{\varphi}_1$, $\alpha_1 \to \bar{\alpha}_1$, $\pi/2 \to -\pi/2$ (see Ref. 9).

Acknowledgments

The authors wish to acknowledge the support of the U.S. Air Force Office of Scientific Research under Contract AFOSR F49620-86-C- 0066, Anthony Amos, technical monitor. The authors also wish to acknowledge the assistance of Christine Chen and Ali Zandieh in the experimental testing.

References

[1]Rainey, G. A., "Preliminary Study of Some Factors Which Affect the Stall-Flutter Characteristics of Thin Wings," NACA TN-3622, March 1956.

[2]Hollowell, S. J., and Dugundji, J., "Aeroelastic Flutter and Divergence of Stiffness Coupled, Graphite/Epoxy Cantilevered Plates,"

Journal of Aircraft, Vol. 21, No. 1, 1984, pp. 69–76.

[3]Selby, H. P., "Aeroelastic Flutter and Divergence of Rectangular Wings with Bending-Torsion Coupling," M.S. Thesis, Dept. of Aeronautics and Astronautics, Massachusetts Inst. of Technology, Cambridge, MA, Jan. 1982.

[4]Landsberger, B., and Dugundji, J., "Experimental Aeroelastic Behavior of Unswept and Forward Swept Graphite/Epoxy Wings," *Journal of Aircraft,* Vol. 22, No. 8, 1985, pp. 679–686.

[5]Tran, C. T., and Petot, D., "Semi-Empirical Model for the Dynamic Stall of Airfoils in View of Application to the Calculation of Responses of a Helicopter in Forward Flight," *Vertica,* Vol. 5, No. 1, 1981, pp. 35–53.

[6]Dat, D., and Tran, C. T., "Investigation of the Stall Flutter of an Airfoil with a Semi-Empirical Model of 2-D Flow," *Vertica,* Vol. 7, No. 2, 1983, pp. 73–86.

[7]Peters, D. A., "Toward a Unified Lift Model for Use in Rotor Blade Stability Analyses," *Journal of the American Helicopter Society,* Vol. 30, No. 3, 1985, pp. 32–42.

[8]Petot, D., and Dat, R., "Unsteady Aerodynamic Loads on an Oscillating Airfoil with Unsteady Stall," *Proceedings of 2nd Workshop on Dynamics and Aeroelasticity Stability Modeling of Rotorcraft Systems,* Florida Atlantic Univ., Boca Raton, FL, Nov. 1987.

[9]Dunn, P. E., "Stall Flutter of Graphite/Epoxy Wings with Bending-Torsion Coupling," M.S. Thesis, Department of Aeronautics and Astronautics, Massachusetts Inst. of Technology, Cambridge, MA, May 1989; also TELAC Rept. 89-5, M.I.T., May 1989.

[10]Crawley, E. F., and Dugundji, J., "Frequency Determination and Nondimensionalization for Composite Cantilever Plates," *Journal of Sound and Vibration,* Vol. 72, No. 1, 1980, pp. 1–10.

[11]Meirovitch, L., *Elements of Vibration Analysis,* McGraw-Hill, New York, 1975.

[12]Petot, D., and Loiseau, H., "Successive Smoothing Algorithm for Constructing the Semi-Empirical Model Developed at ONERA to Predict Unsteady Aerodynamic Forces," NASA TM-76681, March 1982.

[13]Jacobs, E. N., and Sherman, A., "Airfoil Section Characteristics as Affected by Variations of the Reynold's Number," NACA Rept. 586, 1937.

[14]Petot, D., "Dynamic Stall Modeling of the NACA 0012 Profile," *Recherches Aérospatiales,* No. 1984-6, pp. 55–58.

[15]Kuo, C.-C., Morino, L., and Dugundji, J., "Perturbation and Harmonic Balance Methods for Nonlinear Panel Flutter," *AIAA Journal,* Vol. 10, No. 11, 1972, pp. 1479–1484.

[16]McAlister, K. W., Pucci, S. L., McCroskey, W. J., and Carr, L. W., "An Experimental Study of Dynamic Stall on Advanced Airfoil Sections Volume 2: Pressure and Force Data," NASA TM-84245, Sept. 1982.

[17]Wu, J.-C., Kaza, K. V. R., and Sankar, J. N., "Technique for the Prediction of Airfoil Characteristics in Separated Flow," *Journal of Aircraft,* Vol. 26, No. 2, 1989, pp. 168–177.